Title No. 115-S65

Seismic Performance Limitations and Detailing of Slender Reinforced Concrete Walls

by Christopher L. Segura Jr. and John W. Wallace

Recent earthquakes and laboratory tests have revealed code-compliant slender walls are vulnerable to brittle compression failure prior to achieving deformation levels allowed in U.S. codes and standards. To identify and address potential deficiencies in current provisions, seven half-scale ACI 318-14-compliant wall specimens were subjected to reversed cyclic lateral loads and constant axial load. Abrupt loss of lateral strength and a large reduction in axial capacity occurred at plastic rotations as low as 0.011 radians for the thinnest walls (6 in. [152 mm]). Plastic rotations greater than 0.025 radians were measured for walls that were 25% and 50% thicker, and/or constructed with confinement detailing exceeding ACI 318-14 requirements. Based on experimental results, it is suggested to improve the deformation capacity of thin walls by avoiding the use of crosstie confinement and by providing transverse reinforcement for web longitudinal reinforcement within the plastic hinge region.

Keywords: boundary element; compression failure; confinement; detailing; instability; reinforced concrete; shear wall; structural wall; wall thickness.

INTRODUCTION

Field observations of slender wall behavior following the 2010 Maule earthquake in Chile and the 2011 Christchurch earthquake in New Zealand—both in locations where seismic design codes similar to those used in the United States have been adopted—demonstrated the potential for code-compliant walls to experience brittle compression failures. Studies conducted following the earthquake in Chile revealed that damage occurred primarily in newer buildings, which were likely to contain walls that were taller, thinner, and designed for larger axial stress demands than typical designs of previous decades (Massone et al. 2012). It is anticipated that a similar trend toward less-conservative designs has occurred in the United States in the past few decades as engineers have sought to produce more economical designs, spurred by advances in structural modeling capabilities, less-conservative design approaches/provisions, and other factors (for example, use of higher-strength concrete). Of particular importance is the fact that it is now standard practice in many parts of the world, including the United States, to construct rectangular walls and walls composed of rectangular sections (T-shape, I-shape, C-shape), although recent laboratory tests on ACI 318-compliant rectangular walls (Nagae et al. 2012; Lowes et al. 2012) and rectangular boundary element specimens (Arteta 2015; Welt 2015) have demonstrated the inability of relatively long, thin rectangular sections to remain stable when subjected to compression yielding. The laboratory tests presented in this paper were conducted to assess issues that led to observed poor wall performance, to identify potential deficiencies in current ACI 318 design provisions, and to make recommendations for reinforcement detailing in the plastic hinge region of slender walls.

RESEARCH SIGNIFICANCE

ACI 318-14 assumes that code-allowable drift limits can be achieved for slender walls if ACI 318 provisions are satisfied; however, recent findings have demonstrated that code-compliant walls may fail prematurely in compression. It is vital to understand the performance limitations of code-compliant walls so that they can be addressed in future ACI 318 code releases. Based on results of large-scale tests and analysis of the test data, recommendations are made for detailing in the plastic hinge region of slender walls.

EXPERIMENTAL INVESTIGATION

Overview

The experimental investigation consisted of subjecting seven, approximately half-scale, wall panel specimens to reversed cyclic lateral forces and constant axial load. The wall panels represented approximately the bottom 1.5 stories of an eight-story cantilever wall. For all seven walls, the applied axial load was $0.10A_{cv}f_c'$ and peak shear stress was approximately $2.5\sqrt{f_c'}$ (psi) $(0.2\sqrt{f_c'}$ [MPa]).

Cross-sectional geometry and reinforcement details of the test specimens are shown in Fig. 1, and overall dimensions are shown in Fig. 2. Six of the walls had a rectangular cross section and the other wall (WP4) had a T-shape cross section with an enlarged boundary region at one end of the wall. The specimens were constructed with a footing and thickened top cap to connect to the laboratory strong floor and to apply actuator loads to the specimens. The test region for all seven specimens was 90 in. (2286 mm) in length and 84 in. (2134 mm) in height. Longitudinal reinforcement was continuous over the full height of the specimens and was anchored into footings and top caps. Design concrete compressive strength f_c' and steel reinforcement yield strength f_y were 5 and 60 ksi (34.5 and 414 MPa), respectively. Average test day material properties are summarized in Tables 1 and 2.

The experimental test matrix is provided in Table 3. Except at the flange boundary of Specimen WP4, the boundary

ACI Structural Journal, V. 115, No. 3, May 2018.
MS No. S-2017-207, doi: 10.14359/51701918, was received June 7, 2017, and reviewed under Institute publication policies. Pertinent discussion including author's closure, if any, will be published ten months from this journal's date if the discussion is received within four months of the paper's print publication.

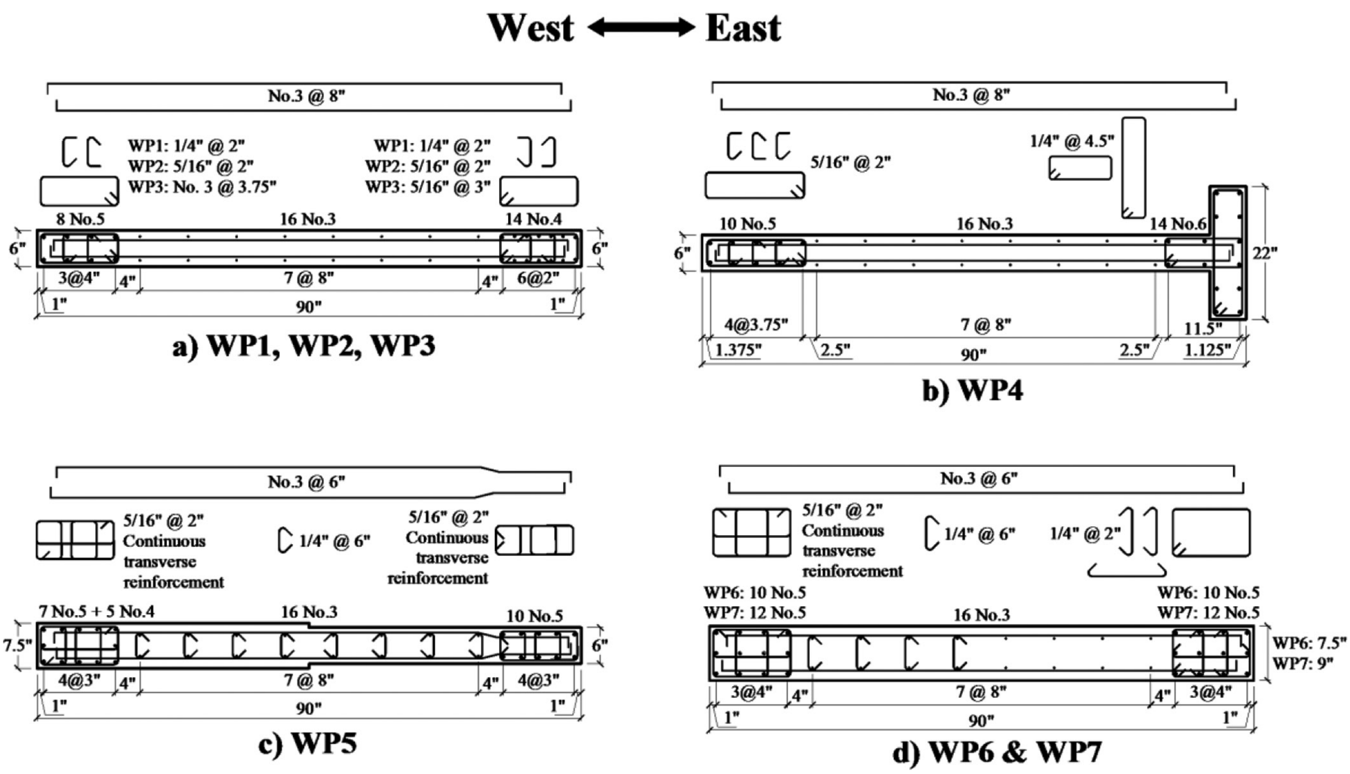

Fig. 1—Reinforcement layout: (a) Specimens WP1, WP2, and WP3; (b) Specimen WP4; (c) Specimen WP5; and (d) Specimens WP6 and WP7. (Note: 1 in. = 25.4 mm.)

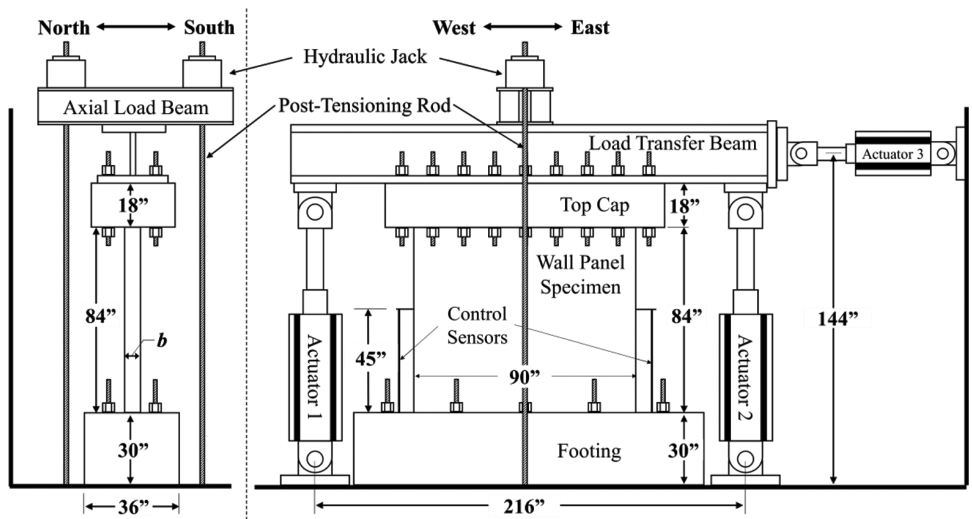

Fig. 2—Test setup. (Note: 1 in. = 25.4 mm.)

regions at the edges of all seven walls were well-confined with transverse reinforcement quantity A_{sh} and spacing s satisfying ACI 318-14 special boundary element detailing. For all seven walls, the arrangement of longitudinal and/or transverse reinforcement was different at the two boundaries; therefore, Table 3 includes information for the west and east boundaries of each specimen. Specimen WP1 was the reference specimen. Specimen WP2 was constructed with approximately 20% more boundary transverse reinforcement A_{sh} than WP1. For Specimen WP3, the spacing of boundary transverse reinforcement was increased, compared to WP1, such that the ratio of transverse reinforcement spacing to longitudinal bar diameter s/d_b was 6 at both boundaries, as compared to $s/d_b = 3.2$ and $s/d_b = 4$ at the west boundary and east boundary of WP1, respectively. Specimen WP4 was designed for a compression depth, determined for an extreme fiber compressive strain of 0.003 (consistent with ACI 318-14 requirements) and axial load of $0.10A_{cv}f_c'$, equal to 30% of the length of the wall ($c = 0.30l_w$) as compared to $c \approx 0.20l_w$ for the other six walls. Specimens WP1 to WP4 were all 6 in. (152 mm) thick and were constructed with a single outer hoop and 90- to 135-degree crossties (indicated as 'HCT 90°-135°' in Table 3) as confinement at wall boundaries. Specimens WP6 and WP7 were 25% and 50% thicker than WP1 (b = 7.5 in. [WP6]; b = 9 in. [WP7]) and were each constructed with a single outer hoop

Table 1—Reinforcement material properties

	Bar size	d_b, in. (mm)	A_b, in.^{2} (mm^2)	$f_{y,test}$, ksi (MPa)	f_u, ksi (MPa)	ε_u	f_{rup}, ksi (MPa)	ε_{rup}
(1)	(2)	(3)	(4)	(5)	(8)	(9)	(10)	(11)
WP1 WP2 WP3 WP4	1/4 in.	0.252 (6.4)	0.05 (32.2)	48.9 (337)	58.5 (403)	0.059	31.0 (214)	0.075
	5/16 in.	0.319 (8.1)	0.08 (51.6)	58.9 (406)	69.8 (481)	0.057	—	—
	No. 3	0.375 (9.5)	0.11 (71.3)	83.9 (578)	105.3 (726)	0.103	85.8 (592)	0.134
	No. 4	0.500 (12.7)	0.20 (127)	73.4 (506)	107.8 (743)	0.111	102.5 (707)	0.142
	No. 5	0.625 (15.9)	0.31 (198)	77.0 (531)	107.6 (742)	0.111	78.6 (542)	0.154
	No. 6	0.750 (19.1)	0.44 (285)	76.9 (530)	104.8 (723)	0.138	81.2 (560)	0.186
WP5 WP6 WP7	1/4 in.	0.252 (6.4)	0.05 (32.2)	70.6 (487)	86.8 (598)	0.092	52.1 (359)	0.096
	5/16 in.	0.319 (8.1)	0.08 (51.6)	63.7 (439)	77.1 (531)	0.071	34.5 (238)	0.103
	No. 3	0.375 (9.5)	0.11 (71.3)	65.8 (454)	102.4 (706)	0.124	85.3 (588)	0.167
	No. 4	0.500 (12.7)	0.20 (127)	74.1 (511)	105.5 (728)	0.138	77.4 (534)	0.163
	No. 5	0.625 (15.9)	0.31 (198)	70.9 (489)	97.1 (669)	0.143	64.9 (447)	0.169

Notes: $f_{y,test}$ is measured yield strength; f_u is measured tensile strength; ε_u is measured strain at tensile strength; f_{rup} is measured rupture strength; ε_{rup} is measured rupture strain.

Table 2—Concrete cylinder material properties

Specimen	Cylinder maturation, days	$f_{c,test}'$, ksi (MPa)	ε_{co}
(1)	(2)	(3)	(4)
WP1	23	5.19 (35.8)	0.0028
WP2	45	6.05 (41.7)	0.0026
WP3	62	6.14 (42.4)	0.0026
WP4	76	6.67 (46.0)	0.0030
WP5	117	6.95 (47.8)	0.0028
WP6	147	6.71 (46.3)	0.0026
WP7	187	7.04 (48.6)	0.0031

Notes: $f_{c,test}'$ is measured cylinder compression strength; and ε_{c0} is measured strain at peak cylinder strength.

and 135-135-degree crossties (HCT 135°-135°) at the east boundary. At the west boundary of WP6 and WP7, a larger quantity of A_{sh} was provided and confinement consisted of continuous transverse reinforcement (CTR), which is similar to overlapping hoops. Specimen WP5 was 6 in. (152 mm) thick over one-half the length of the wall and 7.5 in. (191 mm) over the other half. Continuous transverse reinforcement was used at both boundaries of WP5 and A_{sh} was the largest of all the specimens. For Specimens WP1 to WP4, web longitudinal reinforcement was placed outside of web transverse reinforcement (Fig. 1(a) and 1(b)). In contrast, web longitudinal reinforcement was placed inside transverse reinforcement for Specimens WP5 to WP7 such that longitudinal bars were laterally restrained at a spacing of $16d_b$. In addition, 135-135-degree crossties were used in the web of Specimen WP5 (Fig. 1(c)) and over half the length of the web in Specimens WP6 and WP7 (Fig. 1(d)).

Test setup, loading protocol, and instrumentation

The test setup is shown in Fig. 2. Loading was applied using two vertical actuators, one horizontal actuator, and two hydraulic jacks. The vertical actuators applied a moment couple to the top of the wall panels, and the horizontal actuator applied shear and additional overturning moment. The applied base moment-to-shear ratio (M_b/V_b), reported in Table 3 for each specimen, was constant throughout the tests and was chosen to produce the shear force and moment distribution given by the ASCE 7-10 Equivalent Lateral Force Procedure at the bottom of an eight-story wall with constant story height and story mass up the height of the wall. Most of the axial load was applied by the two hydraulic jacks, and the remainder was applied using the two vertical actuators. An out-of-plane restraint system was used to restrict out-of-plane movement at the top of the specimens.

Figure 3(a) provides details of external instrumentation used to measure wall deformations. Each test specimen was instrumented with approximately 50 linear variable differential transducers (LVDTs) used to measure wall lateral deformations, axial (flexural) deformations, shear deformations, sliding and uplift of specimen footings, and out-of-plane movement of specimen top caps. Strain gauges were mounted to boundary and web longitudinal and transverse reinforcement. A typical layout of strain gauges used to measure boundary transverse reinforcement strains is shown in Fig. 3(b). Cyclic lateral loading was applied by controlling wall rotation, measured by two vertical control sensors positioned at opposite ends of the wall (Fig. 3(a)). The control sensors measured wall rotation over an assumed plastic hinge length equal to one-half the length of the wall ($l_w/2$ = 45 in. [1143 mm]). Figure 4 shows the loading history applied to the specimens. The point at which a 20% reduction in lateral strength was first observed is indicated for each specimen.

EXPERIMENTAL RESULTS

Experimentally measured base moment and shear versus hinge rotation responses for each specimen are presented in Fig. 5. Positive loading corresponds to loading causing compression at the west boundary of the walls. For each specimen, the ASCE 41 (ASCE/SEI 2013) moment versus hinge rotation backbone is included for comparison. The slope of the elastic branch of the ASCE 41 backbone was determined using an effective cracked stiffness of $0.5E_cI_g$.

Table 3—Test variables and boundary reinforcement details

Specimen/ boundary		Primary test variable	b, in. (mm)	Axial load, kip (kN)	$h_{eff} = M_b/V_b$, ft (m)	Confinement detail	$A_{sh1}/A_{ACI}{}^*$	$A_{sh1}/A_{ACI}{}^\dagger$	s/d_b	$c/l_w{}^*$	$c/l_w{}^\dagger$
(1)	(2)	(3)	(4)	(5)	(6)	(7)	(8)	(9)	(10)	(11)	(12)
WP1	West	Reference specimen	6.0 (152)	270 (1201)	28.1 (8.56)	HCT 90°-135°	1.02	0.80	3.2	0.21	0.23
	East								4.0	0.20	0.22
WP2	West	A_{sh}	6.0 (152)	270 (1201)	28.1 (8.56)	HCT 90°-135°	**1.24**	**1.00**	3.2	0.21	0.22
	East								4.0	0.20	0.21
WP3	West	s/d_b	6.0 (152)	270 (1201)	28.1 (8.56)	HCT 90°-135°	1.21	1.38	**6.0**	0.21	0.21
	East						1.09	0.87		0.20	0.20
WP4	West	c/l_w	6.0 (152)	270 (1201)	44.0 (13.4)	HCT 90°-135°	1.23	0.91	3.2	**0.30**	**0.30**
	East					Refer to Fig. 1	—	—	—	**0.06**	**0.07**
WP5	West	Boundary detail	7.5 (191)	338 (1503)	26.8 (8.17)	**CTR**	2.05	1.57	3.2	0.20	0.17
	East		6.0 (152)	270 (1201)						0.21	0.19
WP6	West	b	**7.5 (191)**	338 (1503)	26.8 (8.17)	CTR	1.64	1.30	3.2	0.20	0.18
	East					HCT 135°-135°	1.02	0.90			
WP7	West	b	**9 (229)**	405 (1802)	26.3 (8.03)	CTR	1.64	1.24	3.2	0.20	0.18
	East					HCT 135°-135°	1.02	0.85			

*Determined using nominal material properties.

†Determined using test-day material properties.

Notes: A_{sh1} is area of transverse reinforcement in direction perpendicular to wall length; A_{ACI} is area of transverse reinforcement required by ACI 318-14; h_{eff} is effective height (shear span) equal ratio of base moment (M_b) to base shear (V_b); HCT is single outer hoop and crossties (90- or 135-degree crosstie hook indicated); CTR is continuous transverse reinforcement; 1 in. = 25.4 mm.

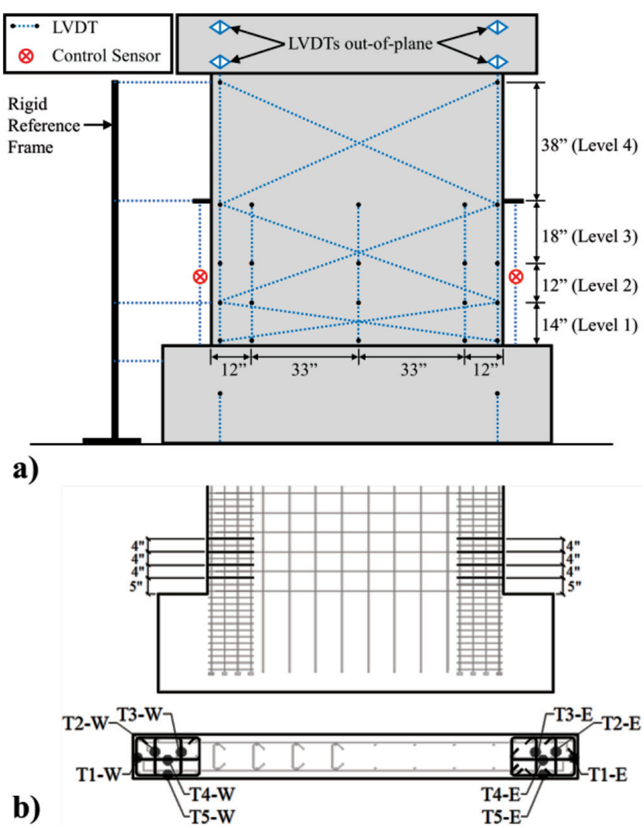

Fig. 3—Instrumentation layout: (a) external instrumentation; and (b) typical layout of strain gauges on boundary transverse reinforcement for Specimens WP5 to WP7.

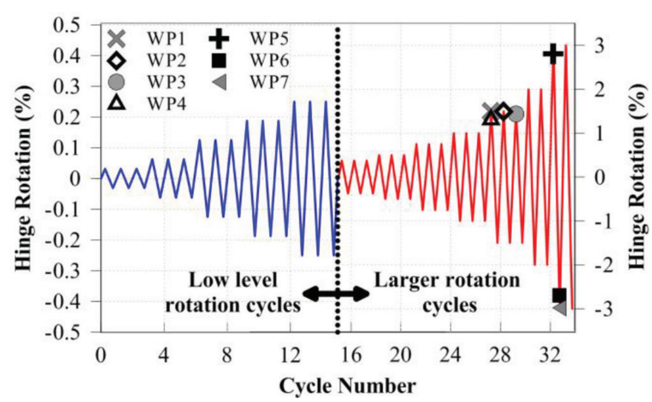

Fig. 4—Applied loading history. Markers indicate first point at which lateral strength dropped at least 20% from peak strength.

The nominal flexural strength was calculated for an extreme fiber compression strain of 0.003 (consistent with ACI 318-14 requirements) and the applied axial load (Table 3) using measured reinforcement and concrete (test-day) properties. Table 4 provides a summary of the measured hinge rotation and base overturning moment for loading in both directions at four points: 1) horizontal flexural cracking of concrete at wall boundaries; 2) first yield of boundary longitudinal reinforcement (determined from strain gauge data); 3) peak strength; and 4) strength loss (determined at the largest rotation for which lateral strength exceeded 80% of peak strength). Additionally, the lateral drift ratio at the effective loading height (δ_u/h_{eff}) is approximated at strength loss for each of the walls. The effective height is defined herein as the ratio of the base overturning moment-to-shear

Table 4—Experimental results summary

	Loading direction	Flexural strength	Cracking		Yielding		Peak load		Strength loss		
		M_n, kip-ft (kN·m)	θ, %	M/M_n	θ, %	M/M_n	θ, %	M/M_n	θ, %	δ_u/h_{eff}, %	M/M_n
WP1	Positive	2515 (3409)	0.050	0.41	0.21	0.86	1.26	1.07	1.59	2.02	0.90
	Negative	–2455 (–3329)	–0.057	0.41	–0.20	0.80	–1.46	1.03	–1.97	–2.56	0.86
WP2	Positive	2560 (3471)	0.049	0.44	0.22	0.90	1.35	1.09	1.52	2.16	1.05
	Negative	–2497 (–3385)	–0.053	0.40	–0.20	0.77	–1.41	1.01	–1.79	–2.46	0.85
WP3	Positive	2566 (3479)	0.048	0.35	0.19	0.77	1.38	1.10	1.51	2.10	0.89
	Negative	–2502 (–3392)	–0.050	0.36	–0.19	0.75	–1.38	1.01	–1.52	–1.99	0.90
WP4	Positive	4183 (5671)	0.054	0.28	0.21	0.68	0.91	0.99	1.31	2.03	0.96
	Negative	–3104 (–4208)	–0.060	0.40	–0.21	0.81	–2.90	1.00	–3.07	–3.88	0.85
WP5	Positive	2888 (3916)	0.058	0.34	0.22	0.76	2.02	1.21	2.81	3.50	1.01
	Negative	–2690 (–3647)	–0.049	0.28	–0.22	0.79	–2.02	1.16	–2.03	–2.83	1.14
WP6	Positive	2867 (3887)	0.047	0.33	0.25	0.91	2.99	1.22	3.02	4.08	1.21
	Negative	–2867 (–3887)	–0.037	0.27	–0.22	0.78	–2.03	1.20	–2.69	–3.21	0.97
WP7	Positive	3389 (4595)	0.051	0.29	0.23	0.82	2.67	1.24	3.04	4.23	1.23
	Negative	–3389 (–4595)	–0.044	0.28	–0.22	0.82	–1.79	1.15	–2.98	–3.99	1.03

Notes: M_n is nominal flexural strength; M is measured base moment; θ is measured hinge rotation; δ_u/h_{eff} is ultimate drift at effective height

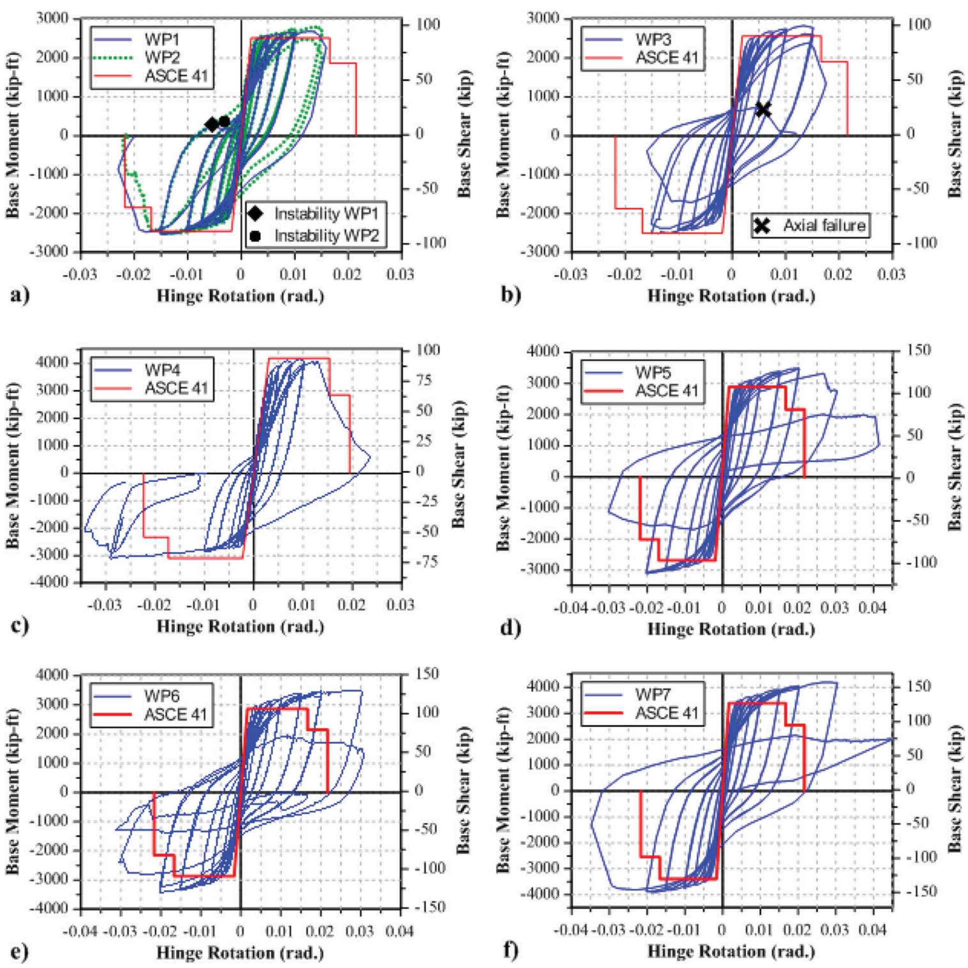

Fig. 5—Base moment and shear versus hinge rotation. (Note: 1 kip = 4.448 kN; 1 kip-ft = 1.356 kN·m.)

($h_{eff} = M_b/V_b$), which is consistent with wall height h_w for a cantilever wall test. The reported δ_u/h_{eff} values include all deformations measured along the panel height, as well as approximate elastic shear and flexural deformations above the wall panel region. A detailed discussion of experimental observations is available in the research report (Segura

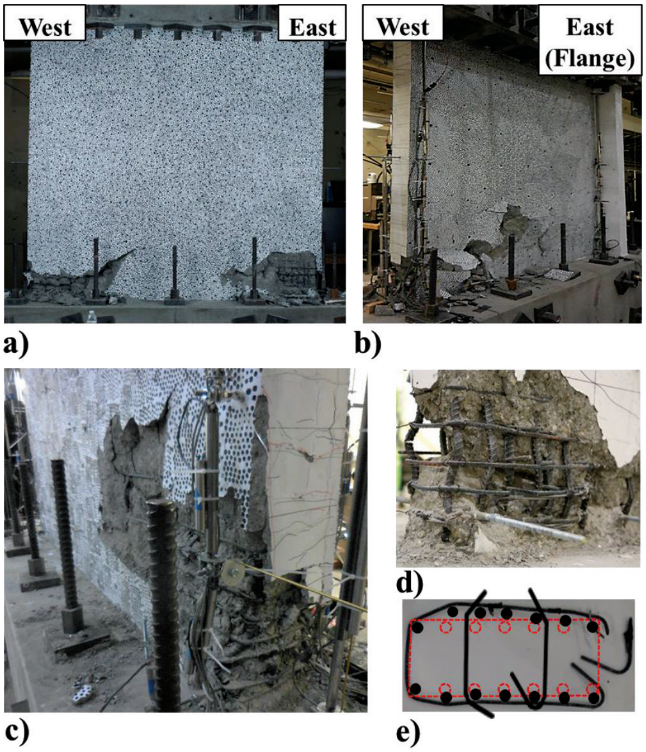

Fig. 6—Observed damage: (a) Specimen WP1 (after test); (b) Specimen WP4 (+1.31%); (c) Specimen WP7 crushing of east boundary and web (–3%); (d) concrete crushing and longitudinal reinforcement buckling at east boundary of WP1; and (e) schematic of crosstie opening and reinforcing bar buckling taken for hoop and crossties removed from WP1 east boundary.

2017), including details about the methods used to estimate δ_u/h_{eff} for each of the specimens.

Photos of typical damage to wall boundaries and web regions are provided in Fig. 6 and 7. The observed behavior was very similar for specimens WP1 and WP2 (Fig. 5(a)), which differed only by the quantity of transverse reinforcement provided at wall boundaries. Both specimens completed three cycles to ±1.0% rotation without strength loss. During loading cycles to +1.5% rotation, crushing and spalling of cover concrete surrounding the confined boundary zones revealed slight buckling of No. 5 longitudinal reinforcement. It is noted that opening of a 90-degree crosstie hook was observed for WP1 in the region where cover spalling occurred. For both walls, out-of-plane instability of the west boundary was observed at a small positive load while reloading to +1.5% rotation (Cycle 2 for WP1 and Cycle 3 for WP2). Because the walls exhibited very little residual lateral strength following the out-of-plane failures (Fig. 5(a)), loading in the positive direction was terminated. While loading monotonically to failure in the negative direction, abrupt compression failure (that is, boundary crushing and longitudinal reinforcement buckling) was observed at the east boundary of WP1 at –1.97% rotation, resulting in nearly instantaneous loss of lateral capacity and a drop in axial load from $0.10A_{cv}f_c'$ (265 kip [1178 kN]) to $0.042A_{cv}f_c'$ (115 kip [510 kN]). A similar failure was observed at the east boundary of WP2 at –1.79% rotation. A photo of the front face of Specimen WP1 immediately after the test is shown in Fig. 6(a).

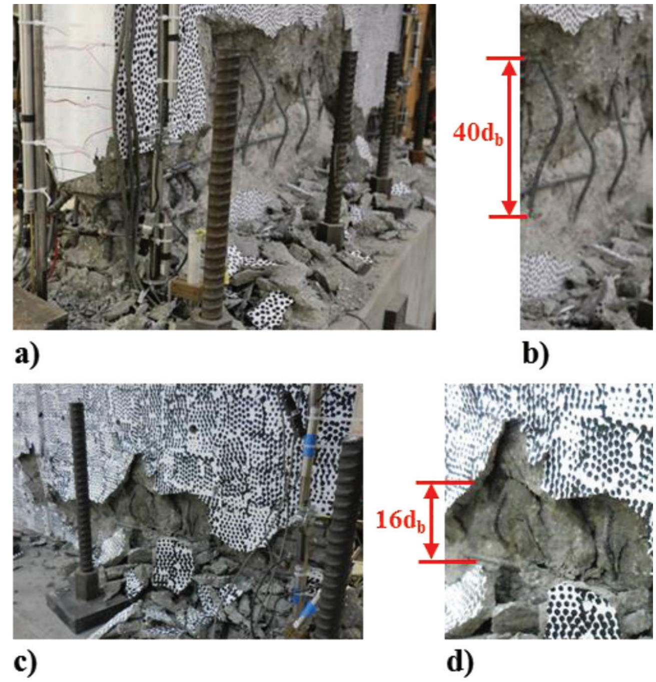

Fig. 7—Damage in web region of specimen: (a) WP3 (end of test); (b) WP3 closeup of buckled longitudinal reinforcement showing buckling over 40d_b; (c) WP5 (–3%); and (d) WP5 closeup showing buckling of longitudinal reinforcement between transverse web reinforcement over height of 16d_b.

For Specimen WP3, which was constructed with wider-spaced boundary transverse reinforcement ($s = 6d_b$) than the other walls, compression failures were observed at both boundaries during loading cycles to ±1.5% rotation. After the third cycle to ±1.5% rotation, an additional cycle was attempted to assess the lateral residual capacity and axial load-carrying capacity of the damaged wall. At approximately +0.6% rotation, crushing occurred along nearly the full length of the wall. Lateral residual strength immediately dropped to near zero (Fig. 5(b)) and the axial load capacity dropped by approximately 60%. Photos of the specimen following the axial failure are shown in Fig. 7(a) and 7(b). Web longitudinal reinforcement was buckled over a height of approximately 12 to 15 in. (305 to 356 mm), or approximately $32d_b$ to $40d_b$. It is noted that web longitudinal reinforcement was placed outside of transverse reinforcement (Fig. 1(a)), a detail that provided no lateral restraint to suppress buckling once concrete crushing/spalling occurred.

For Specimen WP4, different behavior was observed in the two loading directions due to the asymmetric cross section and reinforcement. During the first loading cycle to +1.5% rotation, at a rotation of +1.31%, abrupt crushing of the west boundary and the wall web occurred and the lateral load-carrying capacity abruptly dropped to approximately 15% of the peak capacity. A photo of the front face of the wall following the failure is shown in Fig. 6(b). Damage extended horizontally from the west edge of the wall nearly two-thirds the length of the wall. When loose concrete was removed, it was observed that several No. 3 web longitudinal bars buckled over a height of approximately 15 in. (381 mm [$40d_b$]). While loading in the negative direction, no sign of strength loss was evident at –3% rotation. An additional cycle was performed in the negative direction, during which all No. 5 longitudinal bars at the west boundary ruptured in tension. The test was terminated at –3.5% rotation, at which time the lateral residual capacity in the negative loading direction was approximately two-thirds of the peak capacity. Following the test, damage at the east boundary (flange) consisted of only minor crushing and spalling of cover concrete.

Specimen WP5, which was constructed with continuous transverse reinforcement in the confined boundary regions, completed two cycles to ±2.0% rotation prior to strength loss. At the east boundary, which was 6 in. (152 mm) thick, slight buckling of longitudinal reinforcement was observed at –2.0% rotation (Cycle 2). In the following half load cycle, three of the previously buckled longitudinal bars at the east boundary ruptured in tension, causing an 18% drop from peak strength at +3.0% rotation. While loading in the negative direction to –3.0% rotation, the east boundary (compression zone) began to slide out-of-plane, apparently due to the eccentricity caused by rupture of longitudinal reinforcement and asymmetric crushing/spalling of concrete. Loading was terminated in the negative direction at –3.0% rotation, with a residual capacity of 36% of peak strength. Photos of the wall, taken from the east boundary, are shown in Fig. 7(c) and 7(d). Buckling of web longitudinal bars occurred between transverse bars, over a height of $16d_b$, which was less than half the buckled length of web bars typically observed for Specimens WP1 to WP4 (Fig. 7(a) and 7(b)).

For Specimen WP6, which was 7.5 in. (191 mm) thick, buckling of longitudinal reinforcement was observed at both boundaries during loading cycles to ±2.0% and ±3.0% rotation. Strength loss occurred while loading to –3.0% rotation due to rupture of previously buckled tension reinforcement at the west boundary and concrete crushing and reinforcing bar buckling at the east boundary. In both loading directions, a small number of wide flexural cracks (larger than 0.25 in. [6.4 mm] in width) opened near the base of the wall during loading cycles to ±3.0% rotation, and additional longitudinal bars ruptured in tension in the proceeding cycles. Residual strength of approximately 40% of peak strength was measured in both loading directions at 3% rotation. For Specimen WP7, which was the thickest wall (9 in. [229 mm]), strength loss initiated at –2.98% rotation due to abrupt crushing of the east boundary and wall web. The failure caused an immediate drop in strength to less than 40% of peak capacity. A photo of the east boundary immediately following the failure is shown in Fig. 6(c). Similar to Specimen WP5, buckling of web longitudinal bars occurred between transverse bars, over a height of $16d_b$. Removal of hoops and crossties in the damaged region revealed that some boundary transverse hoops and crossties fractured; although, like Specimens WP1 to WP4, several crosstie hooks opened and fracture was not observed for those crossties.

DISCUSSION OF RESULTS

For Specimens WP1 to WP4, which were the thinnest walls tested (b = 6 in. [152 mm]), brittle flexure-compression failures occurred at plastic hinge rotations ranging between 0.011 and 0.014 radians. For all four walls, residual lateral strength abruptly fell to near zero and a large reduction in axial strength was observed. For comparison, ASCE 41 modeling parameters indicate that the four specimens will maintain 75% of the nominal flexural capacity up to a plastic rotation of 0.02 radians, which is 1.4 to 1.8 times the measured rotation capacities of Specimens WP1 to WP4. Likewise, the walls would not be expected to meet or exceed the ASCE 7 allowable interstory drift ratio (which is approximately equal to rotation within the bottom story of a cantilever wall) of 0.02 radians for walls in Risk I or II category buildings.

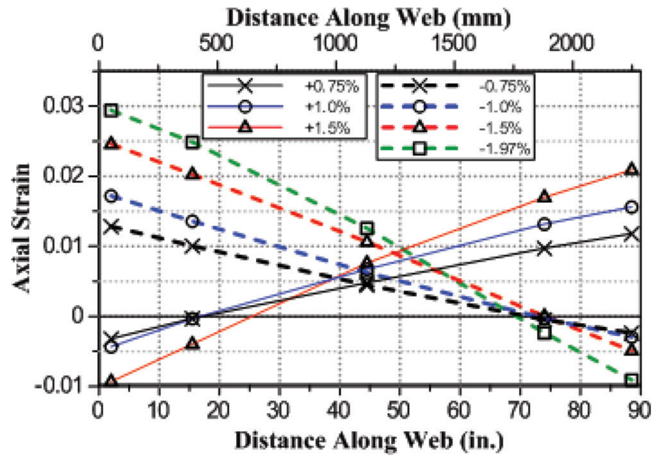

Fig. 8—Specimen WP1 axial strain profiles at various rotation levels.

In Fig. 8, axial strain profiles are shown for Specimen WP1 at various rotation levels. The strain profiles were obtained from columns of vertical sensors at five locations along the length of the wall (Fig. 3(a)). Strains reported in Fig. 8 were measured over Levels 1 through 3, as indicated in Fig. 3(a), with a gauge length of 44 in. (1118 mm) (approximately $l_w/2$). Compression strains measured prior to strength loss were 0.0093 at the west boundary of WP1 (+1.5% rotation) and 0.0091 at the east boundary of WP1 (–1.97% rotation). Maximum compression strains for all seven walls ranged between 0.0077 (WP3 at +1.5% rotation) and 0.012 (WP7 at –2.98% rotation) prior to strength loss. At the boundaries of all walls, softening in the compression zones occurred, and compression strains concentrated over a short height near the base of the walls. Figure 9(a) demonstrates this behavior at the east boundary of Specimen WP1. Average compression strain measurements versus base overturning moment are shown over two different heights above the specimen footing: Level 1 as indicated in Fig. 3(a) (0 to 14 in. [0 to 356 mm]), where inelastic compression strains concentrated, and Levels 2 through 3 (14 to 44 in. [356 to 1118 mm]). The strain reported in Fig. 8 is the average strain over these two heights (0 to 44 in. [0 to 1118 mm]) and is included in Fig. 9(a) for comparison. Initial softening near the base of the wall (0 to 14 in. [0 to 356 mm]) was observed following compression yielding of longitudinal reinforcement at approximately –0.25% rotation, corresponding to an average compression strain of approximately 0.002. At larger

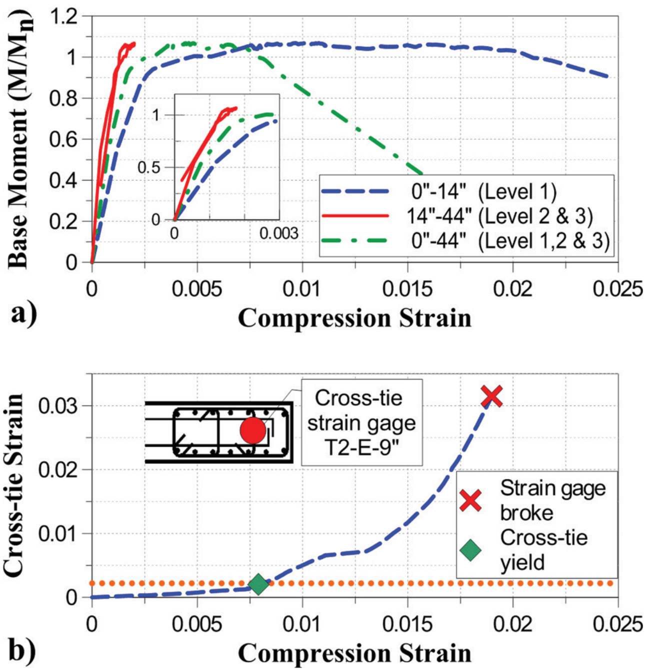

Fig. 9—Specimen WP1 east boundary: (a) normalized base moment versus extreme fiber compression strain (negative loading); and (b) crosstie strain versus axial compression strain in damaged zone (negative loading).

rotation demands, all inelastic compression strain developed in the softened region, and strain unloading occurred above the softened region as strength loss occurred. Prior to failure, sensors in the softened region measured compression strains just below 0.025, while compression strains measured in the sensors above the softened region did not exceed 0.002 at any point in the test. It is noted that inelastic compression strains concentrated over a height of approximately 1.5 to 2.5 times the thickness of the walls (that is, Level 1), which is in agreement with observations from tests conducted on isolated boundary element specimens subjected to uniform compression (Arteta 2015; Welt 2015). However, measured compression strains within the damaged region of boundary element specimens ($\varepsilon_{cu} \approx 0.01$) with similar quantities and configuration of boundary transverse reinforcement have been observed to be substantially lower than the extreme fiber compression strains measured over Level 1 for the walls reported herein ($\varepsilon_{cu} > 0.02$).

Figure 9(b) compares the measured axial compression strains in the softened region (Level 1: 0 to 14 in. [0 to 356 mm]) to transverse strains from a crosstie located at a height of 9 in. (229 mm) above the footing (designated T2-E in Fig. 3(b)). A rapid increase in crosstie strain was observed as axial strains concentrated in the softened region. Crosstie strains exceeding 0.03 were measured just before the strain gauge broke at –1.87% rotation. Figures 6(d) and 6(e) depict the behavior leading to the abrupt compression failure at the east boundary of Specimen WP1. Buckling of all boundary longitudinal reinforcement, generally over multiple hoop spacings, is apparent in Fig. 6(d). It was observed that several hoops fractured in the short, damaged region of the walls; however, fracture of crossties was limited. As indicated by the schematic in Fig. 6(e), it was observed that spalling of cover concrete allowed the 90-degree crosstie hooks to open, making them relatively ineffective in providing confinement and inhibiting longitudinal reinforcement buckling. As the hooks opened, buckling of longitudinal reinforcement was primarily resisted in flexure by the long, flexible hoop legs, which ultimately fractured. As noted earlier, opening of 90-degree crosstie hooks was observed following crushing and spalling of cover concrete. Opening of 135-degree crosstie hooks was also observed in a few cases.

For Specimens WP1 and WP2, failures associated with out-of-plane instability of the compression zone were observed. In Fig. 10(a), the axial strain history at the west boundary of WP1 is shown over the bottom 44 in. (1118 mm) of the wall on the front (north) and rear (south) faces of the specimen. Throughout the test, average axial strains were nearly identical on the front and rear faces of the wall (Fig. 10(a)). However, as shown in Fig. 10(b), in the region where concrete crushing and reinforcing bar buckling was observed (0 to 14 in. [0 to 356 mm]), axial compression strains were significantly different on the two sides of the wall. As a result, out-of-plane rotation occurred in the short, damaged region (0 to 14 in. [0 to 356 mm]) of the wall (Fig. 10(c)). Out-of-plane lateral drift of the specimen top cap (Fig. 10(c)) was nearly equal in magnitude to the out-of-plane rotation measured in the damaged region (0 to 14 in. [0 to 356 mm]) because out-of-plane behavior was concentrated at the base of the wall. Photos of significant damage states are shown in Fig. 10(d) and indicated in Fig. 10(c). The first sign of substantial out-of-plane rotation coincided with vertical cracking and spalling of concrete on the southwest corner of the wall at +0.5% rotation. In the following cycles, an increase in out-of-plane rotation was evident at peak compression points (indicated by markers in Fig. 10(c)) because damage was primarily concentrated on the south face of the wall. At +1.5% rotation, crushed concrete on the north face spalled off and slight buckling of the two longitudinal bars at the west face of the wall was observed. The out-of-plane failure was observed in the following cycle, with out-of-plane rotation occurring primarily over two or three hoop spacings at the location where buckling of longitudinal reinforcement initiated in the previous cycle. Previous studies on lateral instability of thin walls (Paulay and Priestley 1993; Chai and Elayer 1999) have explored a "global buckling" mode by which out-of-plane deformations occur over a significant height (that is, plastic hinge length), influenced by slenderness h/b and inelastic tension strain demand ε_{tu}. It is noted that the east boundary of Specimen WP5, which was the same thickness and height as WP1 and WP2 (h/b = 14), remained stable even though the tension strain demand for WP5 (ε_{tu} = 0.045) was nearly double that of WP1 and WP2 (ε_{tu} < 0.03). Thus, instabilities for WP1 and WP2 were likely influenced primarily by asymmetric crushing/spalling of concrete and buckling of longitudinal reinforcement. Detailed studies conducted following the 2010 earthquake in Chile indicate that this instability mode, initiated by concrete crushing, was likely the cause for instability in many walls in Chile (NIST 2014). It is noted that a minimum wall thickness requirement ($b \geq h/16$) was added to ACI 318-14, which all seven test specimens satisfied. Based

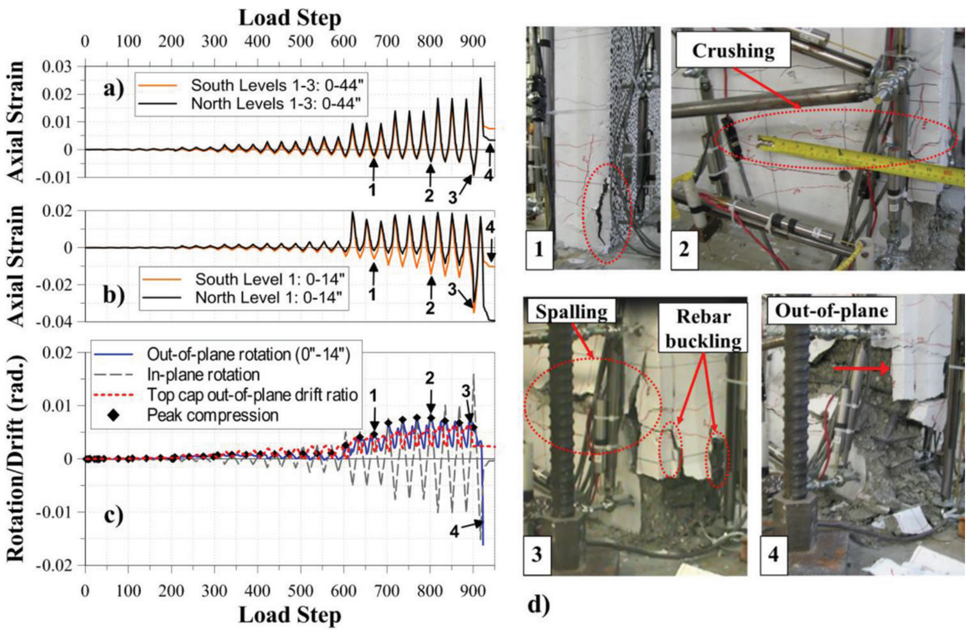

Fig. 10—Specimen WP1 west boundary out-of-plane behavior: (a) average axial strain over 0 to 44 in.; (b) axial strain in damaged zone (0 to 14 in.); (c) out-of-plane rotation in damaged zone; and (d) damage states (1) vertical cracking and spalling on southwest corner (+0.5% rotation), (2) minor cover crushing on north face (+1.0% rotation), (3) cover spalling and reinforcing buckling (+1.5% rotation, cycle 1), and (4) out-of-plane instability. (Note: 1 in. = 25.4 mm.)

on the performance of WP1 and WP2, it may be necessary to modify the wall thickness requirement to account for additional variables such as drift demand.

Specimens WP5 to WP7 were able to achieve inelastic rotations between 0.018 radians (WP5) and 0.028 radians (WP7) prior to strength loss, which are approiximately 1.3 and 2.0 times the rotation capacity of WP1, respectively. Stable buckling of longitudinal reinforcement was observed at the boundaries of WP6 and WP7. In contrast, rapid loss of strength was observed following initial bar instability for the 6 in. (152 mm) thick walls, including WP5 (east boundary). For WP1 to WP4, slight buckling of longitudinal reinforcement was accompanied by abrupt crushing of the confined section or out-of-plane instability. The enhanced confinement detail for WP5 (that is, continuous transverse reinforcement) prevented compression failure, and the slightly buckled bars ruptured in tension in the following half load cycle. Test results for WP5 demonstrated moderately improved deformation capacity; however, it is noted that the quantity of boundary transverse reinforcement A_{sh} was twice the amount required by ACI 318-14 (Table 3), and continuous boundary reinforcement (similar to overlapping hoops) was used. The improved compression behavior for WP5 agrees with findings from isolated boundary element specimen tests (Welt 2015), in which it was shown that ductile compression behavior is achievable in thin sections constructed with overlapping hoop confinement, no crossties, and substantially more A_{sh} than required by ACI 318-14. Thus, although it may be possible to improve the deformation capacity of thin walls, the quantity of the boundary transverse reinforcement required may not be practical or economical. On the other hand, even greater improvement in deformation capacity was achieved by increasing wall thickness (WP6 and WP7) without increasing A_{sh} or using continuous transverse reinforcement.

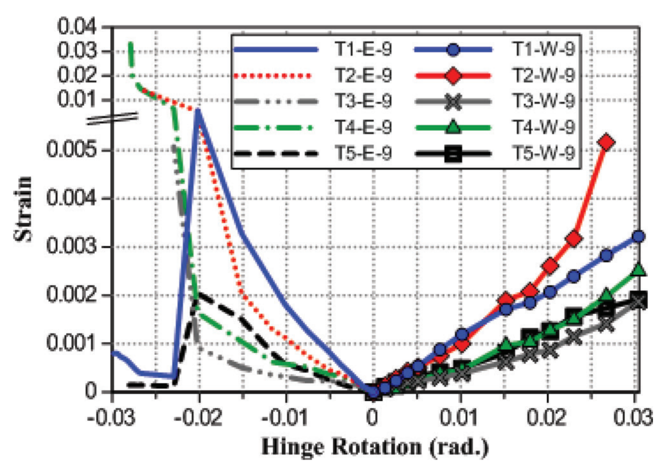

Fig. 11—Specimen WP7 boundary transverse reinforcement strains versus hinge rotation.

Figure 11 compares strain measurements for transverse reinforcement at the east and west boundaries of Specimen WP7 at various rotation levels. The reported strains in Fig. 11 were measured on transverse reinforcement located at a height of 9 in. (229 mm) above the footing (Fig. 3), the height at which transverse strains were largest. In the negative loading direction, causing compression at the east boundary (hoop and crosstie detail), strain Gauge T1-E-9 (hoop strain at the east boundary height of 9 in. [425 mm] above footing) reached yield strain at approximately –1.2% rotation, and strain gauge T2-E-9 (crosstie) reached yield at approximately –1.7% rotation. Beyond –2.0% rotation, a rapid increase in crosstie strains (Gauges T2-E-9, T3-E-9, and T4-E-9) occurred, which may be attributed to bar instability, which was first observed at –2.0% rotation. In the positive loading direction, causing compression at the west boundary (continuous transverse reinforcement detail), transverse strains were smaller for a given rotation level, even though axial compression strains were nearly identical in the two loading directions. Based on Fig. 11, it appears transverse strains became disproportionately large at the locations of crossties at the boundary with the hoop and crosstie detail, whereas the continuous transverse reinforcement detail appears to provide more uniformly distributed transverse strains.

SUMMARY AND CONCLUSIONS

Experimental results were presented for seven half-scale slender wall panel specimens representing approximately the bottom 1.5 stories of an eight-story cantilever wall. Based on the test results, the following observations and conclusions are made:

1. Experimental results for test specimens representing full-scale, 12 in. (305 mm) thick walls indicate thin walls may fail in compression prior to achieving the lateral drift or rotation capacities assumed by ASCE 7 and ASCE 41, respectively, even though the walls satisfy ACI 318-14 provisions. Plastic rotation capacities as low as 0.011 radians were measured for the thinnest walls tested (b = 6 in. [152 mm]), followed immediately by a drop in lateral load capacity to near zero. Walls that were 25% and 50% thicker (7.5 and 9 in. [191 and 229 mm]) were able to achieve plastic rotations greater than 0.025 radians prior to strength loss. Based on test observations, it is apparent that equivalent performance is not expected for all walls that satisfy ACI 318-14 Special Structural Wall requirements. Further study is required to determine how to address drift capacity limitations for thin walls in future building codes and specifications.

2. Abrupt compression failure was observed for walls using a single outer hoop and crossties for confinement. Strain gauge data indicated crosstie strains become disproportionately large in comparison to hoops once crushing/spalling of cover concrete occurs, leading to rapid degradation of the compression-resisting mechanism. In contrast, compression failure was not observed at boundaries of walls confined by continuous transverse reinforcement, which is similar to overlapping hoops. Continuous transverse reinforcement, and presumably overlapping hoops, enable more uniform distribution of transverse strains, providing more stable confinement than a single hoop with crossties.

3. For two of the walls presented (WP1 and WP2), premature strength loss occurred due to out-of-plane instability of the compression zone following concrete crushing/spalling and initial buckling of longitudinal reinforcement, even though the slenderness ratio (h/b = 14) for these walls was less than the maximum allowed by ACI 31-14 ($h/b \leq 16$). Thicker walls (WP6 and WP7) demonstrated greater stability in compression at similar or larger compression strain demands, indicating that it may be necessary to modify the requirements for minimum wall thickness in ACI 318-14 to include additional variables, such as drift demand. The data presented for the approximately half-scale walls suggests that walls designed for moderate compression demands (c/l_w = 0.2 to 0.3) may necessitate at least a 15 to 18 in. (381 to 457 mm) thick compression zone. A review of a larger database of laboratory tests may help to better define a minimum wall thickness and to further study the impact of compression depth and confinement detail on lateral stability.

4. Fracture of crossties was only observed in a few cases for the tests reported in this paper. Instead, following crushing and spalling of cover concrete, 90-degree crosstie hooks opened, making them less effective in providing confinement and resisting longitudinal bar buckling. Very little, if any, performance enhancement was observed for crossties with 135-degree hooks on each end. It is suggested to avoid the use of a boundary element with a single hoop and crossties, and to use overlapping hoops or continuous transverse reinforcement for boundary transverse reinforcement. This approach may be conservative for some walls, and further research is necessary to determine the design parameters (that is, wall geometry, compression depth, drift demand) for which a single hoop with crossties detail may be sufficient.

5. ACI 318-14 allows web longitudinal reinforcement to be placed outside of transverse reinforcement with no requirement for lateral restraint by crossties. For walls designed with this detail (WP1 to WP4), buckling of web longitudinal reinforcement was observed over heights up to approximately $40d_b$ and the walls were unable to maintain lateral residual strength and axial load following compression failure at approximately 1.5% rotation. For walls in which longitudinal bars were laterally restrained at $16d_b$ (WP5 to WP7), residual lateral strength greater than approximately 40% of peak capacity was maintained to at least 3% rotation. Lateral restraint for longitudinal web reinforcement using crossties is recommended in the plastic hinge region to maintain residual strength and protect against axial failure.

AUTHOR BIOS

ACI member **Christopher L. Segura Jr.** *was formerly a PhD Student at the University of California, Los Angeles (UCLA), Los Angeles, CA. He is now a Research Structural Engineer at the National Institute of Standards and Technology. He received his BS and MS from the University of Colorado, Boulder, CO. He is a member of ACI Committees 133, Disaster Reconnaissance, and 369, Seismic Repair and Rehabilitation. His research interests include seismic design and laboratory testing of reinforced concrete structures.*

John W. Wallace, *FACI, is a Professor of civil engineering at UCLA. He is a member of ACI Committees 318, Structural Concrete Building Code; 369, Seismic Repair and Rehabilitation; 374, Performance-Based Seismic Design of Concrete Buildings; and ACI Subcommittee 318-H, Seismic Provisions. His research interests include response and design of buildings and bridges to earthquake actions, laboratory and field testing of structural components and systems, and seismic structural health monitoring.*

ACKNOWLEDGMENTS

The work presented in this paper was supported by funds from the National Science Foundation (NSF) Grant No. CMMI-1208192. The reported experiments were conducted in a laboratory renovated with funds provided by the NSF under Grant No. 0963183. This financial support is gratefully acknowledged. The authors would like thank UCLA laboratory engineers S. Keowen, A. Salamanca, H. Kasper, and E. Ahlberg; NEES REU participants A. Flintrop, M. Shea, J. Guitierrz, and S. Herrera; and UCLA students A. Yu, D. Thomas, M. Daciolas, R. Mahmoudzadeh, and C. Motter for their assistance conducting the experiments. Any opinions, findings, and conclusions or recommendations expressed in this material are those of the authors and do not necessarily reflect the views of others mentioned here.

NOTATION

A_{cv} = gross area of concrete bounded by web thickness and length
A_{sh} = total cross-sectional area of transverse reinforcement (including crossties) within spacing s and perpendicular to member core dimension b_c, measured to outside edges of transverse reinforcement
b = width of compression face
c = distance from extreme compression fiber to neutral axis
c_c = clear cover to outside edge of reinforcement
d_b = nominal diameter of bar
E_c = modulus of elasticity of concrete
f_c' = specified compressive strength of concrete
f_y = specified yield strength of reinforcement
I_g = moment of inertia of gross concrete section about centroid axis, neglecting reinforcement
l_w = length of wall in direction of shear force
s = center-to-center spacing of transverse reinforcement

REFERENCES

ACI Committee 318, 2014, "Building Code Requirements for Structural Concrete (ACI 318-14) and Commentary (ACI 318R-14)," American Concrete Institute, Farmington Hills, MI, 520 pp.

Arteta, C. A., 2015, "Seismic Response Assessment of Thin Boundary Element Specimens of Special Concrete Shear Walls," PhD dissertation, University of California, Berkeley, Berkeley, CA, 240 pp.

ASCE/SEI, 2010, "Minimum Design Loads for Buildings and Other Structures (ASCE/SEI 7-10)," American Society of Civil Engineers, Reston, VA, 608 pp.

ASCE/SEI, 2013, "Seismic Rehabilitation and Upgrade of Existing Buildings (ASCE/SEI 41-13)," American Society of Civil Engineers, Reston, VA, 518 pp.

Chai, Y. H., and Elayer, D. T., 1999, "Lateral Stability of Reinforced Concrete Columns under Axial Reversed Cyclic Tension and Compression," *ACI Structural Journal*, V. 96, No. 5, Sept.-Oct., pp. 780-789.

Lowes, L. N.; Lehman, D. E.; Birely, A. C.; Kuchma, D. A.; Marley, K. P.; and Hart, C. R., 2012, "Earthquake Response of Slender Planar Concrete Walls with Modern Detailing," *Engineering Structures*, V. 43, pp. 31-47. doi: 10.1016/j.engstruct.2012.04.040

Massone, L. M.; Bonelli, P.; Lagos, R.; Lüders, C.; Moehle, J.; and Wallace, J. W., 2012, "Seismic Design and Construction Practices in RC Structural Wall Buildings," *Earthquake Spectra*, V. 28, pp. S245-S256. doi: 10.1193/1.4000046

Nagae, T.; Tahara, K.; Fukuyama, K.; Matsumori, T.; Siohara, H.; Kabeyasawa, T.; Kono, S.; Nishiyama, M.; Moehle, J.; Wallace, J.; Sause, R.; and Ghannoum, W., 2012, "Test Results of Four-Story Reinforced Concrete and Post-Tensioned Concrete Buildings: The 2010 E-Defense Shaking Table Test," *Proceedings of the 15th World Conference on Earthquake Engineering*, Lisbon, Portugal, 234 pp.

NIST, 2014, "Recommendations for Seismic Design of Reinforced Concrete Wall Buildings Based on Studies of the 2010 Maule, Chile Earthquake," NIST GCR 14-917-25, NEHRP Consultants Joint Venture, National Institute of Standards and Technology, Gaithersburg, MD, 322 pp.

Paulay, T., and Priestley, M. J. N., 1993, "Stability of Ductile Structural Walls," *ACI Structural Journal*, V. 90, No. 4, July-Aug., pp. 385-392.

Segura, C. L., 2017, "Seismic Performance Limitations and Reinforcement Detailing of Slender RC Structural Walls," PhD dissertation, University of California, Los Angeles, Los Angeles, CA, 238 pp.

Welt, T. S., 2015, "Detailing for Compression in Reinforced Concrete Wall Boundary Elements: Experiments, Simulations, and Design Recommendations," PhD dissertation, University of Illinois, Urbana-Champaign, IL, 530 pp.

NOTES: